JPE 16-6-28

http://dx.doi.org/10.6113/JPE.2016.16.6.2284
ISSN(Print): 1598-2092 / ISSN(Online): 2093-4718

A Novel Multi-Function PV Micro-Inverter with an Optimized Harmonic Compensation Strategy

Guofeng Zhu*, Longhua Mu†, and Junhua Yan*

*†College of Electronics and Information Engineering, Tongji University, Shanghai, China

Abstract

With the rapid development of clean energy, photovoltaic (PV) generation has been utilized in the harmonic compensation of power systems. This paper presents a novel multi-function PV micro-inverter with three stages (pseudo-two-stage). It can inject active power and compensate harmonic currents in the power grid at the same time. In order to keep the micro-inverter working under the maximum allowable output power, an optimized capacity limitation strategy is presented. Moreover, the harmonic compensation can be adjusted according to the customized requirements of power quality. Additionally, a phase shedding strategy in the DC/DC stage is introduced to improve the efficiency of parallel Boost converters in a wide range. Compared with existing capacity limitation methods, the proposed strategy shows better performance and energy efficiency. Simulations and experiments verify the feasibility of the micro-inverter and the effectiveness of the strategy.

Key words: PV, micro-inverter, harmonic compensation, capacity limitation, phase shedding

I. INTRODUCTION

With the gradual depletion of fossil energy and the increasing deterioration of the environment, the study of renewable energy, represented by solar energy and wind power, has become a hot topic worldwide. Due to the price decline of PV modules and the development of global PV markets, the cost of PV power systems continues to go down [1]-[3]. PV power systems are gradually showing their competitiveness.

For grid-connected PV systems, a centralized PV inverter is conventional equipment for PV modules interfacing with the electricity network [4]. In this approach, PV modules are first divided into series connections and then into parallel [5]. Although this kind of inverter can reach high power levels, it has obvious drawbacks. When some PV modules are faulty or when partially shading occurs, the mismatch losses between the PV modules significantly influence the efficiency of the whole PV system. Some methods have been presented to optimize the maximum power point tracking (MPPT) algorithm and to detect PV module faults [6], [7]. A virtual MPPT scheme combined with thermographical fault diagnosis is proposed to improve efficiency under partial shading conditions [8]. A micro-inverter, also called a cell inverter or an ac-module inverter, integrates an inverter and a single PV module into one electrical device [9], [10]. Since every PV module has its own individual MPPT, a PV power system can achieve a relative high energy efficiency even under partial faulty or partial shading conditions. In addition, the characteristics of "Plug and Play" operation and good expandability make the micro-inverter suitable for low-power level conditions, such as the Roof Program and some building integrated PV (BIPV) projects [11]-[14].

Meanwhile, with the extensive application of power electronic devices and other nonlinear loads in distribution networks, power quality problems have become serious [15]. Capacitors and passive harmonic filters are typical passive power quality conditioners with simple features and a low cost. Moreover, active power quality conditioners, such as the active power filter (APF), dynamic voltage regulator (DVR) and unified power quality conditioner (UPQC), with their more flexible strategies and controllable functions, can achieve better performance in power quality conditions. Because of the difference between ideal and practical working environments, many PV inverters work under the conditions that are below the rated output power in the daytime. The remaining capacity of these inverters can be

Manuscript received Jan. 26, 2016; accepted Jun. 18, 2016
Recommended for publication by Associate Editor Yihua Hu.
†Corresponding Author: lhmu@tongji.edu.cn
Tel: +86-21-59949122, Fax: +86-21-69589870, Tongji University
*College of Electronics and Information Eng., Tongji University, China

used for other functions. Since some active power quality conditioners have a structure that is similar to that of PV inverters in the DC/AC stage, some researchers have tried to multiplex them to achieve multi-function [16]-[19]. Wu T.F. et al. have designed a single-phase PV system, which can provide real power injection and harmonic current compensation at the same time [16]. He J.W. et al. have presented a voltage-control-based DG-grid inverter with harmonic compensation [17]. The method is flexible and cooperates well with *V-f* droop controlled DG systems. He J.W. et al. have also proposed an enhanced current-control DC unit, which can achieve harmonic compensation without using any local harmonic extraction or harmonic voltage detection at the point of connection (POC) [18]. A flexible power controller based on the single-phase *p-q* theory is developed, which can improve the controllability of grid-connected multi-functional photovoltaic inverters with advanced features, such as low voltage ride-through and reactive power compensation [19].

Generally, the primary task for a PV inverter is to inject active power current into the grid while the secondary task is to compensate harmonic currents with the remaining capacity. However, the requirements of harmonic compensation for power grid always go far beyond the capacity of an inverter, particularly micro-inverters. If the output current exceeds the allowable value of an inverter, the device can be damaged. For safety, the capacity for the harmonic compensation of an inverter must be limited. In order to control the output current, an amplitude clamping algorithm (ACA) and an amplitude scaling algorithm (ASA) have been proposed [21]. However, an inverter needs to identify the load-type first and then determine which algorithm should be utilized. Furthermore, the ACA will introduce new harmonic currents to the grid. Zeng Z. et al. have proposed a coordinated control strategy based on the Fryze-Buchholz-Dpenbrock (FBD) theory [22]. By limiting the harmonic and reactive conductance and susceptance, the inverters can cooperate in accordance with their capacities without communication. However, the computational process of this strategy is too complicated to apply in electricity networks with complex topologies.

In this paper, a novel multi-function micro-inverter with three stages (pseudo-two-stage) is presented. Focusing on the capacity limitation problem of micro-inverters, an optimized harmonic compensation strategy is proposed. By controlling the scaling factor of every harmonic order individually, the limited compensation capacity can be utilized more effectively. Moreover, the strategy can customize the allocation factor of the compensation capacity according to the requirements of power quality. Compared with existing methods, the proposed strategy is customizable and easier to apply. In addition, a phase shedding control for parallel Boost converters in the DC/DC stage is presented to improve the efficiency of the converter under light and heavy loads.

Section II introduces the topology of the PV micro-inverter. Section III presents the control structure of the multi-function micro-inverter. An optimized capacity allocation strategy with a better compensation effect is also proposed. Section IV introduces parallel Boost converters in the DC/DC stage and efficiency optimization with phase shedding control. Then, a prototype of the micro-inverter is built. Simulation and experimental results are presented in Section V. Finally, some conclusions are given in Section VI.

II. Topology of the Multiple-Stage Micro-Inverter

The topologies of PV inverters can be classified on the basis of the numbers of power processing stages, the location of the power decoupling capacitors and the type of the transformers [4]. A single-stage inverter should achieve voltage amplification, MPPT, output current shaping and galvanic isolation functions all in one stage [23], [24]. The fly-back topology is a common topology with a relatively simple structure and control strategy [2], [25]. For a single-stage micro-inverter, it has to step up the low voltage of a single PV module significantly to match the utility level. It is a challenge to achieve high efficiency and multiple functions with large turn ratios. For a two-stage micro-inverter, a cascade connection of a step-up DC/DC converter and a grid-tied high-frequency inverter is a typical design [26], [27]. Since multiple-stage micro-inverters have more stages than other types, more control algorithms and functions can be applied individually [28], [29]. They can have better performance with various optimal control strategies.

This paper proposes a micro-inverter with three stages (pseudo-two-stage) as shown in Fig. 1. The first stage is a double parallel Boost converter, which performs MPPT and raises the DC voltage to 48V. The second stage is a fly-back converter. The output current of this stage is modified to follow a rectified wave including fundamental and harmonic signals. The third stage is a full bridge converter to unfold the rectified current at low switching frequencies. Then the current passes through a passive LC filtering circuit and connects to the grid.

Since the multi-stage micro-inverter has more components than others, improving the energy efficiency and reducing the product cost are challenging issues. In addition to the disadvantages mentioned above, this topology has the following advantages:

1) Since the output voltage of the PV module has a wide range, the efficiency of the DC/DC converter is influenced. With the optimal phase shedding control presented in Section IV, the parallel Boost converters can improve efficiency when the output of photovoltaic fluctuates.

2) Compared with single-stage inverters, multiple-stage

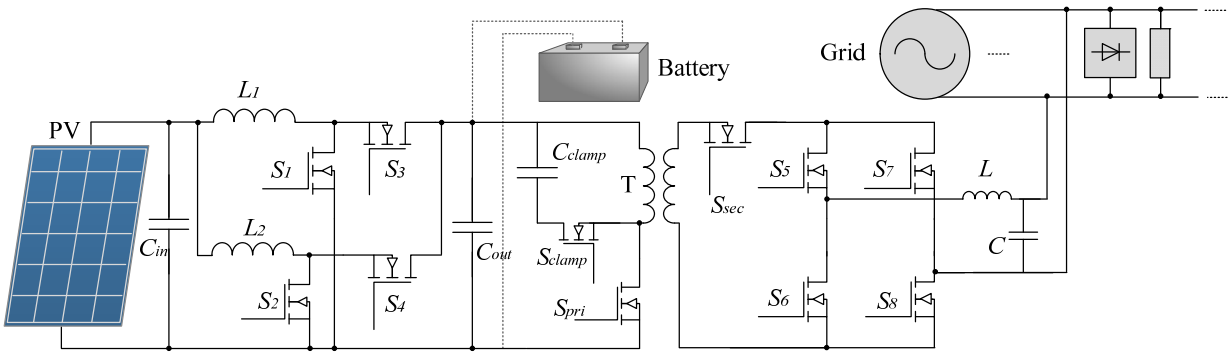

Fig. 1. Topology of the multiple-stage micro-inverter for single PV module.

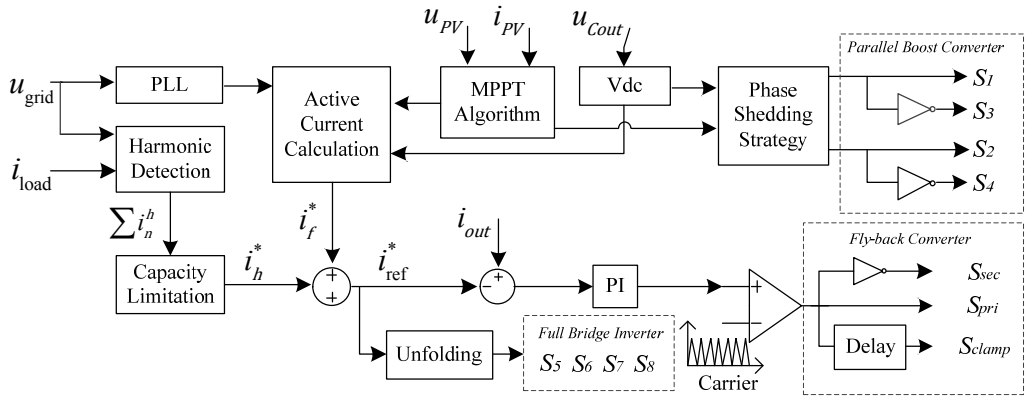

Fig. 2. Control block of the multi-function inverter.

inverters have individual control tasks for each stage. Therefore, they can provide more room to optimize the control algorithm.

3) The fly-back converter is suitable for low-power applications. It also can provide electrical isolation at the same time. As a result, there is no need to put a power frequency transformer in the micro-inverter.

4) By using active clamping technology for the fly-back converter and zero current transition (ZVT) method for a full bridge converter, the switching loss can be reduced.

5) This micro-inverter is expandable and suitable for residential distribution networks. It can become a PV-Battery hybrid system by accessing an energy storage device after the parallel Boost converters (the grey part "Battery" in Fig. 1). Then, more functions and operation modes can be developed.

III. Control of Harmonic Current Compensation

A. Control Structure of the Multi-Function Micro-Inverter

A control block diagram of the multi-function micro-inverter is shown in Fig. 2. The Output current of the micro-inverter includes active power injection and harmonic compensation.

The desired value of the active power current i_f^* is calculated by the MPPT and the voltage of the capacitor C_{out}. By detecting the harmonic currents in the grid and combining them with the maximum value of the allowable output current of the micro-inverter, the desired value of the output harmonic compensating current i_h^* can be calculated. Then the desired output current i_{ref}^* can be described as Equ. (1).

$$i_{ref}^* = i_f^* + i_h^* \tag{1}$$

Modulated by the absolute rotary and the SPWM block, the control signal of the fly-back converter can be generated.

Based on the deviation between the desired output current i_{ref}^* and the actual output current i_{out}, the desired output voltage u_{out} can be calculated.

$$u_{out} - u_{\text{grid}} = \frac{L}{\Delta T}(i_{ref}^* - i_{out}) \tag{2}$$

where u_{grid} is the voltage of the grid, L is the inductance of the output inductor, and ΔT is the sampling time.

By tracking the zero crossing point of the desired output current, the power switches of the full bridge converter can be controlled.

B. Harmonic Current Detection

In three-phase power systems, instantaneous reactive power theory has been widely used to detect harmonic signals [30]. For single-phase systems, a virtual synchronous frame conversion of the measured signals needs to be constructed [31]. To reduce the computational burden and complexity, this paper has applied a high-performance harmonic

extraction algorithm [32]. By multiplying the sine and cosine functions of the chosen frequency and filtering by a low pass filter, the target components in the measured signals can be extracted, as shown in Fig. 3.

For example, the measured signal i_{load} contains fundamental and nth harmonic components as:

$$i_{load} = I_0 \cos(\omega_0 t + \theta_0) + I_n \cos(n\omega_0 t + \theta_n) \quad (3)$$

Multiplied by $\cos(n\omega_0 t)$, the signal can be expressed as:

$$i_{c1} = \frac{I_0}{2}[\cos(\omega_0 t + \theta_0 + n\omega_0 t) + \cos(\omega_0 t + \theta_0 - n\omega_0 t)] + \frac{I_n}{2}[\cos(2n\omega_0 t + \theta_n) + \cos(\theta_n)] \quad (4)$$

After a low pass filter is added, the signal is multiplied by $\cos(n\omega_0 t)$ a second time:

$$i_{c2} = i_{cl}\cos(n\omega_0 t) = \frac{I_n}{2}\cos(\theta_n)\cos(n\omega_0 t) \quad (5)$$

Finally, i_n^h is the nth harmonic component extracted in i_{load}.

$$\begin{aligned} i_n^h &= 2(i_{c2} + i_{s2}) \\ &= 2[\frac{I_n}{2}\cos(\theta_n)\cos(n\omega_0 t) - \frac{I_n}{2}\sin(\theta_n)\sin(n\omega_0 t)] \\ &= I_n \cos(n\omega_0 t + \theta_n) \end{aligned} \quad (6)$$

Compared with the commonly used harmonic filtering approaches, this algorithm is simpler and easier to apply to the controllers.

C. Capacity Limitation

For PV systems, the weather condition directly affects the output power of a PV module. When the sunlight is abundant, the output power of a PV module may approximate its rated value. On the contrary, if the sunlight is weak or blocked, the output power of a PV module is less than its rated value and the remaining capacity for harmonic compensation is sufficient. However, in practical conditions, most micro-inverters are low-power and the requirements of harmonic compensation for power grids always exceed the capacity of a single PV micro-inverter. For safety, a limitation on the capacity for harmonic compensation is necessary.

For a convenient analysis, Fig. 4 shows the harmonic compensating current with different limitation algorithms. The gray line (i_{total}) represents the compensating current without a limitation. The orange line (I^h_{max}) represents the amplitude of the maximum allowable harmonic compensating current. The black line (i_{ACA}) and green line (i_{ASA}) represent compensating currents with the ACA and ASA algorithms, respectively. The red line (i_{ASA*}) is the compensating current with different scaling factors for each harmonic order. In low-voltage distribution networks, the low-frequency odd harmonics are prominent and the amplitudes of the high-frequency harmonics are relative small. The compensated harmonic currents in this paper only include the

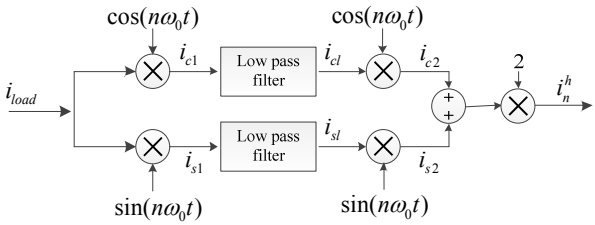

Fig. 3. Control block of harmonic extraction.

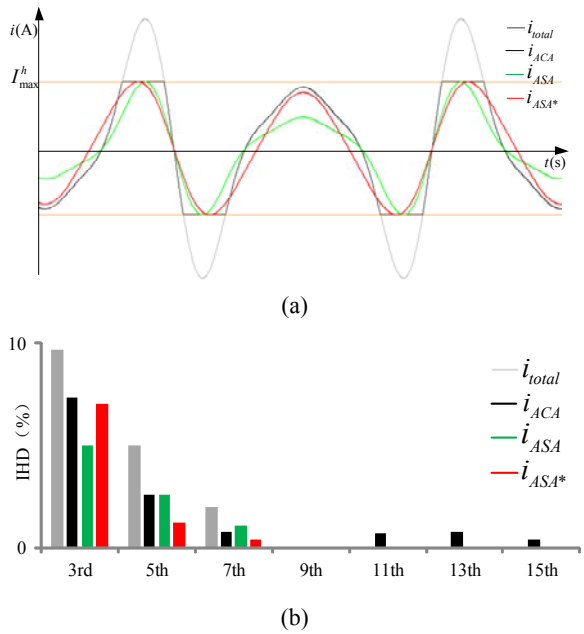

Fig. 4. Comparison of compensating current with different limitation methods. (a) Waveforms of compensating current. (b) Harmonic components of compensating current.

3rd, 5th and 7th order.

Since i_{total} represents the compensating current without a limitation, it can be derived as:

$$i_{total} = \sum_{n=3,5,7} \sqrt{2} I_n \cos(n\omega_0 t + \theta_n) \quad (7)$$

The harmonic compensating current with the ASA algorithm can be expressed as:

$$i_{ASA} = \begin{cases} i_{total}, & 0 < I_{total} \le I^h_{\max} \\ x_{ASA} i_{total}, & I_{total} > I^h_{\max} \end{cases} \quad (8)$$

and:

$$x_{ASA} = \frac{I^h_{\max}}{I_{total}} \quad (9)$$

where I_{total} is the amplitude of the ideal harmonic compensating current without a limitation, and x_{ASA} is the global scaling factor.

When the harmonic compensating current is below the maximum allowable value, there is no need for a limitation. On the contrary, the current should be scaled down according to the global scaling factor.

For the ACA, if the current exceeds the maximum

allowable value, it is clamped at the value of I^h_{max}, as shown in Fig. 4(a).

With the ASA, harmonic compensating currents of every order will be scaled down linearly to fit the rated current value. Even though no additional harmonic current will be generated, the utilization efficiency of the capacity for harmonic compensation is not satisfactory. With the ACA, only the peak current is clamped to the rated value, and the system can achieve a high energy efficiency. Compared with i_{ASA} in Fig. 4, i_{ACA} has a relative higher utilization of the compensating capacity. However, the clamped compensating current includes harmonic components of higher orders. It introduces additional harmonic current to the grid, as shown in Fig. 4(b).

From the above, if the scaling factor of every harmonic order is controlled individually, the capacity for harmonic compensation may be utilized more effectively.

$$i_{ASA^*} = \begin{cases} i_{total}, & 0 < I_{total} \le I^h_{\max} \\ \sum_{n=3,5,7} x_n \sqrt{2} I_n \cos(n\omega_0 t + \theta_n), & I_{total} > I^h_{\max} \end{cases} \quad (10)$$

where x_n is the individual scaling factor for every harmonic order.

Moreover, if the scaling factor cooperates with the customized task of power quality, the effect of harmonic current compensation can be improved at the same time.

D. Optimization of Harmonic Current Compensation

In this paper, the proposed strategy of harmonic current compensation is focused on the following three points:

1) Customization of Power Quality

Different categories of power loads have different requirements for power quality. For example, if power loads have a relative low requirement for harmonic distortion, the capacity for harmonic compensation can be reduced [33]. Therefore, the strategy for harmonic compensation should be adjusted according to the specific power quality demands of the loads. Then, the customization of power quality can be achieved.

2) Optimization of Capacity Allocation

When the capacity for harmonic compensation is limited, the effect of compensation with the ASA is not optimal. This is due to the fact that the ASA allocates compensation capacity on the basis of the same scaling factor to every harmonic order. However, the distortion degree of every harmonic order is different. If the allocation is based on the extent of distortion, a harmonic order with a more serious distortion will be allocated more compensation capacity (the scaling factor of the harmonic order with a more serious distortion will be larger).

3) Simplicity and Practicality

Since a micro-inverter is applied to a single PV module, volume and cost should be taken into account. The control circuit and strategy should be highly efficiency and easy to apply.

This paper proposes an optimized strategy for capacity allocation for harmonic current compensation. In order to ensure the speed and efficiency of the control system, this paper chooses to calculate the amplitude of the maximum allowable harmonic current instead of the maximum allowable capacity. Compared with the complexity of the capacity calculation, the amplitude calculation of the harmonic current is easier to apply. The amplitude of the maximum allowable harmonic compensating current can be expressed as:

$$I^h_{\max} = I_{\max} - I_f \quad (11)$$

where I_f is the amplitude of the active power current injected into the grid, and I_{max} is the amplitude of the maximum allowable output current of the micro-inverter.

The primary task of harmonic compensation is to minimize harmonic distortion and keep the output current of the micro-inverter under an allowable value. Since total harmonic current distortion (THD_I) is an important indicator to measure the effect of harmonic compensation, the relationship can be described as:

$$THD_I = \frac{\sqrt{\sum_{k=3,5,7\ldots} \left|(1-x_k)i^k\right|^2}}{I_f} \quad (12)$$

$$I^h = \left|\sum_{k=3,5,7\ldots} x_k i^k\right| \le I^h_{\max} \quad (13)$$

where i^k is the harmonic current of the kth order, x_k is the scaling factor of the kth order, and $x_k i^k$ is the harmonic compensating current for the kth order.

By solving these two equations at the same time, the optimized scaling factors can be obtained, and optimized harmonic compensation with a minimum of total harmonic distortion under the situation of a capacity limitation can be achieved. However, the operation method is too complicated to utilize in practical applications. Based on the above theories, a simplified operation method is proposed.

By means of harmonic detection, the harmonic current distortion of every order (IHD) can be calculated. Combined with the customized task of power quality, the optimal capacity allocation of harmonic compensation can be achieved. For example, the computational processes of harmonic current compensation for the kth order are shown in Equs. (14)-(16). IHD_k is the kth harmonic current distortion. IHD_k^* is the customized value for the kth harmonic current distortion. ΔIHD_k is the deviation between IHD_k and IHD_k^*.

$$IHD_k = \frac{\sqrt{I_k^2}}{I_f} \times 100\% \quad (14)$$

$$\Delta IHD_k = \begin{cases} IHD_k - IHD_k^* & (IHD_i > IHD_i^*) \\ 0 & (IHD_i < IHD_i^*) \end{cases} \quad (15)$$

Then, the amplitude of the kth harmonic compensating

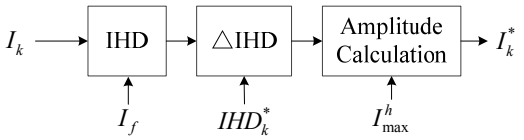

Fig. 5. Control block of capacity limitation.

current can be calculated as:

$$I_k^* = I_{\max}^h \frac{\Delta IHD_k}{\sum_{k=3,5,7...} \Delta IHD_k} \tag{16}$$

Fig. 5 shows a control block of the optimized capacity limitation for harmonic compensation.

For every harmonic order, the greater the deviation of the harmonic distortion when compared with the customized threshold, the more capacity for harmonic compensating current will be allocated. That is to say, the capacity allocation will be proportional to the deviation of every harmonic order. Thus, the limited capacity will put more effort into the primary harmonic distortion orders. When compared with the ASA, both the effect of the harmonic compensation and the efficiency of the energy utilization will be improved. When compared with the ACA, no additional harmonic orders are produced. This strategy does not generate any additional harmonic current pollution.

IV. Efficiency Optimization of the DC/DC Stage

As a general rule, a DC/DC converter is designed according to the rated operation situation. As a result, the efficiency of the converter under light loads and heavy loads will be greatly reduced [34]. Meanwhile, fluctuations in the output power of the PV module affect the efficiency of the DC/DC converter. This paper proposes parallel Boost converters for PV generation systems with the phase shedding strategy. By comparing the actual input current with the phase shedding point, the phase number of the parallel converters can be determined, and the efficiency of the PV power system under light loads and heavy loads can be improved.

A. Efficiency Model of the Boost Converter

Fig. 6 is an equivalent circuit of a Boost converter. In this figure, L and D are the inductor and diode, C_{in} represents the input capacitor, U_s represents the output voltage of the PV model, U_o is the output voltage of the Boost converter, U_{on} is the forward voltage drop of the diode, R_C is the equivalent series resistance of the input capacitor, R_L is the equivalent resistance of the inductor, and R_{on} represents the on-resistance of the power switch.

The efficiency of the converter can be expressed as:

$$\eta = \frac{P_{out}}{P_c + P_s + P_{out}} \tag{17}$$

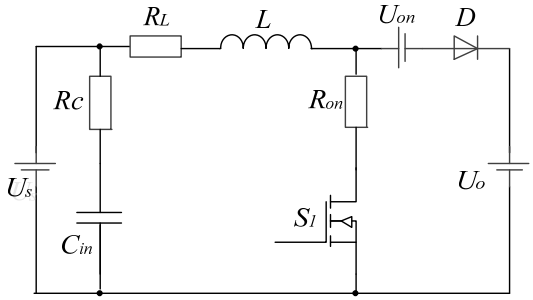

Fig. 6. Equivalent circuit of Boost converter.

where P_{out} is the output power of the Boost converter, P_c represents the conduction loss with consideration of the voltage drop and equivalent impedance, and P_s is the switching power loss of the power switches.

The output power of the Boost converter can be expressed as:

$$P_{out} = (1-d)U_o I_L \tag{18}$$

where d represents the duty ratio, and I_L is the average current of the inductor.

According to the operation characteristics of the Boost converter, P_s can be expressed as:

$$P_s = \frac{(U_o + U_{on})I_L f T_{s1}}{2} + (U_o + U_{on}) \cdot \frac{(U_s - I_L(R_L + R_{on}))d}{4L} T_{s2} \tag{19}$$

$$T_{s1} = t_{cross(off)} + t_{cross(on)} \tag{20}$$

$$T_{s2} = t_{cross(off)} - t_{cross(on)} \tag{21}$$

where f is the switching frequency, and $t_{cross(on)}$ and $t_{cross(off)}$ are the crossover times of the power switch turning-on and turning off.

P_c consists of the voltage drop loss of the diode, the conduction loss of the power switches and the loss of the equivalent resistance in the circuit.

$$P_c = I_L(1-d)U_{on} + dI_L^2 R_{on} + I_L^2 R_L + (I_{in} - I_L)^2 R_c \tag{22}$$

Under the static state, I_{in} is equal to the average current of the inductor I_L.

$$I_{in} = I_L \tag{23}$$

Plugging Equs. (18)-(23) into (17) yields an efficiency model of the Boost converter:

$$\eta = \frac{U_o I_{in}}{\alpha I_{in}^2 + \beta I_{in} + \gamma} \tag{24}$$

where α、β、γ can be expressed as:

$$\alpha = \frac{R_L + dR_{on}}{1-d} \tag{25}$$

$$\beta = U_{on} + U_o + \frac{(U_o + U_{on})fT_{s1}}{2(1-d)} - \frac{(U_o + U_{on})(R_L + R_{on})dT_{s2}}{4L(1-d)} \tag{26}$$

$$\gamma = \frac{(U_o + U_{on})U_s dT_{s2}}{4L(1-d)} \tag{27}$$

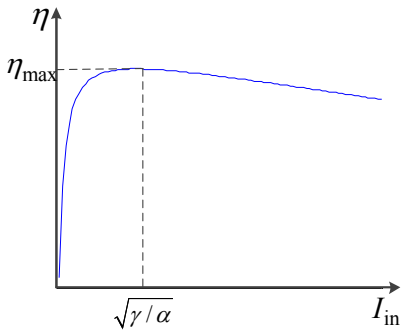

Fig. 7. Expected efficiency-current curve of Boost converter.

B. Phase Shedding Strategy

If the parameters are constant, the efficiency of the converter is only related to the input current. For the Boost converter, first order partial derivatives of the efficiency model can be expressed as:

$$\frac{\partial \eta}{\partial I_{in}} = \frac{U_o(\gamma - \alpha I_{in}^2)}{(\alpha I_{in}^2 + \beta I_{in} + \gamma)^2} \tag{28}$$

Fig. 7 shows the expected efficiency-current curve of the Boost converter. As shown in this figure, the efficiency rapidly increases along with the input current when the current is low. However, when the loads are heavy, the efficiency decreases while the input current increases. Since the output power of a PV module is affected by the environment, the photovoltaic has less time to work at its full-power output. The average efficiency of a photovoltaic generation system is unsatisfactory.

Since parallel converters can extend the working range and reduce the current stress by adjusting the phase number of the parallel converters, the efficiency of the system can be improved [35], [36].

For parallel converters, there is an assumption that all of the parameters of the circuit are the same. Thus, every phase of the parallel converters has the same efficiency model. Since there are two parallel boost converters in the proposed topology, the current in every phase distributes the total current evenly. Referring to Equ. (24), the efficiency model of each phase can be expressed as:

$$\eta(\frac{I_{in}}{2}) = \frac{2U_o I_{in}}{\alpha I_{in}^{\ 2} + 2\beta I_{in} + 4\gamma} \tag{29}$$

According to Equ. (29), the expected efficiency-current curve of the multiphase Boost converters can be drawn as Fig. 8. In this figure, the dotted black line represents a single (one-phase) Boost converter and the dotted red line represents double parallel (two-phase) Boost converters. The solid blue line represents the curve of double parallel Boost converters with the phase shedding strategy. When compared to converters with a constant phase number (one-phase and two-phase), the converters with the phase shedding strategy have a higher efficiency when the loads are light or heavy.

As shown in Fig. 8, P is the phase shedding point. If the input current is less than the point of P, the efficiency of the one-phase Boost converter is higher. On the contrary, two-phase Boost converters have a higher efficiency. Thus, the optimized efficiency model can be expressed as:

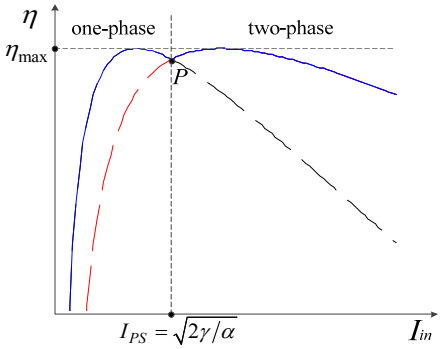

Fig. 8. Expected efficiency-current curve of multiphase Boost converter.

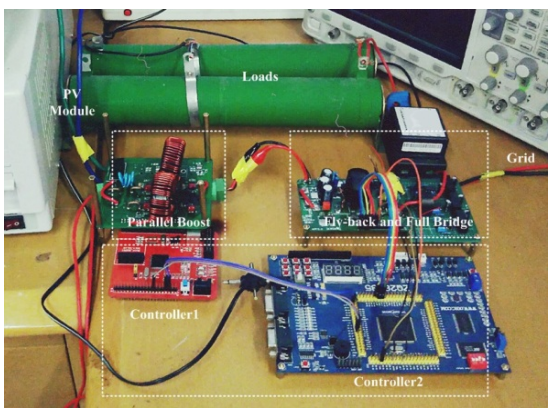

Fig. 9. Prototype of multi-function PV micro-inverter.

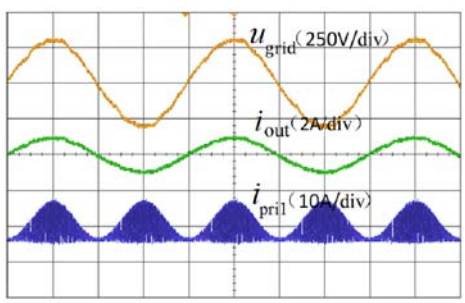

(a)

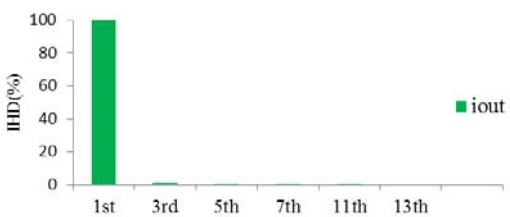

(b)

Fig. 10. Experimental results of micro-inverter with active power injection. (a) Waveforms of the micro-inverter. (b) FFT analysis of i_{out}.

$$\eta_{\max} = \begin{cases} \eta(\frac{I_{in}}{1}), & 0 < I_{in} \le I_{PS} \\ \eta(\frac{I_{in}}{2}), & I_{in} > I_{PS} \end{cases} \quad (30)$$

$$I_{PS} = \sqrt{\frac{2\gamma}{\alpha}} \quad (31)$$

where I_{PS} is the current of the phase shedding point P.

V. Simulation and Experiments

A. Multi-function Micro-Inverter

A 190W experimental prototype of a multi-function micro-inverter has been built, as shown in Fig. 9.

For the fly-back inverter, the power switch of the primary side is an IRFS4321, the clamp switch is a SI7115DN, the power switches of the full bridge are 17N80s, and the master controller is a TMS30F28335. The single PV module is on the roof and it connects to the micro-inverter with electrical wire.

Fig. 10 shows the function of the active power injection by the micro-inverter. u_{grid} is the voltage of the power system. i_{out} is the output current of the micro-inverter and it changes along with u_{grid} in sinusoidal form. i_{pril} is the primary side current of the fly-back converter with the SPWM control.

Fig. 11 shows the multi-function of the active current injection and the harmonic current compensation by the micro-inverter. i_{load} is the load current of the power system caused by non-linear loads. i_{out} is the output current of the micro-inverter, which includes the active power current and harmonic compensating current. i_{grid} is the current of the power grid. With the harmonic current compensation, i_{grid} can be returned to sinusoidal form.

B. Optimized Capacity Allocation

When the capacity for the harmonic compensation is insufficient, the output current for the harmonic compensation should be limited. In order to verify the superiority of the proposed capacity allocation strategy, an experiment has compared it with the ASA. The customized value of the individual harmonic distortion is 3%. The bar charts in Fig. 12 are the harmonic current distortions of the 3rd, 5th and 7th harmonic orders. The blue bar is the harmonic distortion before compensation. The red bar and green bar are the harmonic distortions with the ASA and the proposed strategy, respectively.

Since the harmonic distortion of the 3rd order is the most serious, when compared with the ASA, the system with the proposed strategy has allocated a lot more capacity for the 3rd harmonic current compensation. As a result, the harmonic distortion of every harmonic order is more even. The total harmonic distortion (THD) with the proposed strategy is reduced to 4.38% while the THD with the ASA is 5.52%.

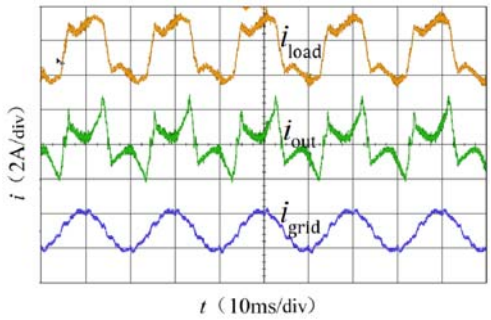

(a)

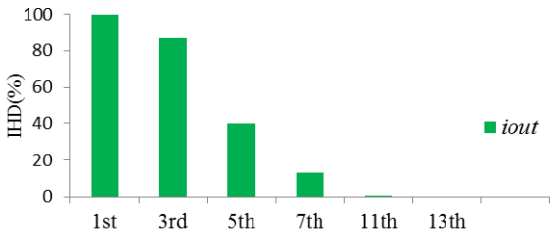

(b)

Fig. 11. Experimental results of micro-inverter with active power injection and harmonic current compensation. (a) Waveforms of the micro-inverter. (b) FFT analysis of i_{out}.

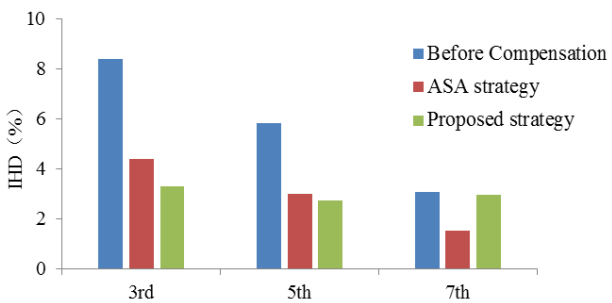

Fig. 12. Harmonic current distortion with compensation.

When compared with the ASA, the proposed strategy has a better and more balanced performance in terms of harmonic current compensation.

C. Phase Shedding Strategy

To verify the phase shedding strategy in the DC/DC stage, several experiments have been carried out. Table I shows the key parameters of the converters.

Regardless of the power loss of the converters, the auxiliary power supply and the drivers, the input and output power can be measured. The efficiency-current curve of the converters can be drawn as shown in Fig. 13. In the figure, the black dot is the efficiency of a one-phase Boost converter, the red dot is the efficiency of two-phase Boost converters, and the blue dot is the efficiency of two-phase Boost converters with the phase shedding strategy. Since the result is consistent with the analysis shown in Section IV, it can be seen that the efficiency, especially under light and heavy loads, of the converters has been improved.

TABLE I
KEY CIRCUIT'S PARAMETERS OF BOOST CONVERTERS

Parameters	Value	Parameters	Value
P_{out}/W	190	R_L /Ω	0.8
U_{out}/V	48	R_C /Ω	0.01
U_s /V	26~38	$t_{cross(on)}$/ns	30
f /kHz	300	$t_{cross(off)}$/ns	50
L/uH	10	U_{on} /V	0.5
C_{out}/uF	47	R_{on} /Ω	0.045

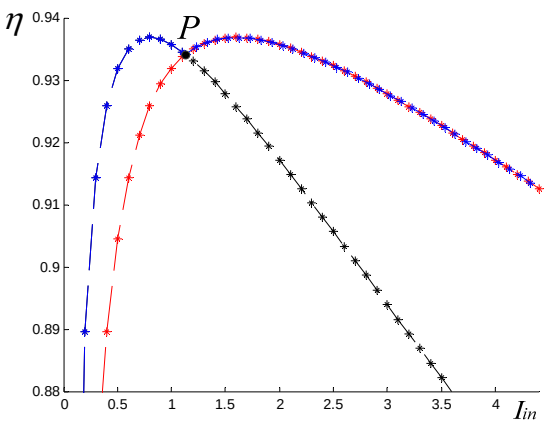

Fig. 13. Efficiency-current curve of converters with phase shedding control.

VI. CONCLUSIONS

This paper proposes a novel multi-function PV micro-inverter with three stages (pseudo-two-stage). It can achieve active current injection and harmonic current compensation at the same time. An optimized limitation strategy for harmonic compensation is proposed. According to the requirements of power quality, the strategy can customize the optimal capacity allocation factor for harmonic current compensation. When compared with existing methods, the proposed strategy has a better efficiency in terms of energy utilization and harmonic compensation performance. Moreover, in the DC/DC stage of the micro-inverter, the phase shedding strategy for parallel Boost converters can maintain a relative high efficiency under light and heavy working conditions. In addition, because of the capacity limitation, the harmonic compensation of a single micro-inverter is suitable for low power applications. For higher power applications, several micro-inverters need to working together to accomplish the task. In such cases, the strategy of coordination control for these micro-inverters requires further study.

REFERENCES

[1] International Energy Agency Photovoltaic Power Systems, *(2015) Trends in photovoltaic applications. Survey report of selected IEA countries between 1992 and 2014*. www.iea-pvps.org, 2015.

[2] Y. H. Hu, W. P. Cao, W. D. Xiao, and B. Ji, "Three-port DC-DC converter for stand-alone photovoltaic systems," *IEEE Trans. Power Electron.*, Vol. 30, No. 6, pp. 3068-3076, Jun. 2015.

[3] F. Nejabatkhah, S. Danyali, S. H. Hosseini, M. Sabahi, and S. M. Niapour, "Modeling and control of a new three-input DC–DC boost converter for hybrid PV/FC/battery power system," *IEEE Trans. Power Electron.*, Vol. 27, No. 5, pp. 2309-2324, May 2012.

[4] S. B. Kjaer, J. K. Pedersen, and F. Blaabjerg, "A review of single-phase grid-connected inverters for photovoltaic modules," *IEEE Trans. Ind. Applicat.*, Vol. 41, No. 5, pp. 1292-1306, Sep. 2005.

[5] M. Calais, J. Myrzik, T. Spooner, and V. G. Agelidis, "Inverters for single-phase grid connected photovoltaic systems-an overview," in *IEEE Power Electronics Specialists Conference (PESC)*, Vol. 4, pp. 1995-2000, Jun. 2002.

[6] B. Subudhi and R. Pradhan, "A comparative study on maximum power point tracking techniques for photovoltaic power systems," *IEEE Trans. Sustain. Energy*, Vol. 4, No. 1, pp. 89-98, Jan. 2013,

[7] Y. H. Hu, B. Gao, X. G. Song, G. Y. Tian, K. J. Li, and X. N. He, "Photovoltaic fault detection using a parameter based model," *Solar Energy*, Vol. 96, pp. 96-102, Oct. 2013.

[8] Y. H. Hu, W. P. Cao, J. D. Wu, B. Ji, and D. Holliday, "Thermography-based virtual MPPT scheme for improving PV energy efficiency at partial shading conditions," *IEEE Trans. Power Electron.*, Vol. 29, No. 11, pp. 5667-5672, Jun. 2014.

[9] R. H. Wills, F. E. Hall, S. J. Strong, and J. H. Wohlgemuth, "The AC photovoltaic module," in *IEEE Photovoltaic Specialists Conference*, pp. 1231-1234, May. 1996.

[10] T. Shimizu, K. Wada, and N. Nakamura, "A flyback-type single phase utility interactive inverter with low-frequency ripple current reduction on the DC input for an AC photovoltaic module system," in *IEEE Power Electronics Specialists Conference (PESC)*, Vol. 3, pp. 1483-1488, Jun. 2002.

[11] Q. Li and P. Wolfs, "A review of the single phase photovoltaic module integrated converter topologies with three different DC link configurations," *IEEE Trans. Power Electron.*, Vol. 23, No. 3, pp. 1320-1333, May, 2008.

[12] Y. Xue, K. C. Divya, G. Griepentrog, M. Liviu, S. Suresh, and M. Manjrekar, "Towards next generation photovoltaic inverters," in *IEEE Energy Conversion Congress and Exposition (ECCE)*, pp.2467-2474, 2011.

[13] B. Jablonska, A. L. Kooijman-van Dijk, H. F. Kaan , M. van Leeuwen, G. T. M.de Boer, and H. H. C. de Moor. "PV-prive project at ECN: five years of experience with small-scale AC module PV systems," in *European Photovoltaic Solar Energy Conference and Exhibition*, Vol. 6, Jun. 2005.

[14] S. Guha, "Can your roof provide your electrical needs?-the growth prospect of building-integrated photovoltaic," in *IEEE Photovoltaic Specialists Conference*, pp: 12-16. Jan. 2005

[15] J. M. Guerrero, P. C. Loh, T. L. Lee, and M. Chandorkar, "Advanced control architectures for intelligent microgrids – Part II: Power quality, energy storage, and AC/DC microgrids," *IEEE Trans. Ind. Electron.*, Vol. 60, No. 4,

pp. 1263-1270, Apr. 2013.
[16] T. F. Wu, H. S. Nien, C. L. Shen, and T. M. Chen, "A single-phase inverter system for PV power injection and active power filtering with nonlinear inductor consideration," *IEEE Trans. Ind. Applicat.*, Vol. 41, No. 4, pp. 1075-1083, Jul. 2005.
[17] J. W. He, Y. W. Li, and M. S. Munir, "A flexible harmonic control approach through voltage-controlled DG–grid interfacing converters," *IEEE Trans. Ind. Electron.*, Vol. 59, No. 1, pp. 444-455, Jan. 2012.
[18] J. W. He, Y. W. Li, F. Blaabjerg, and X. Wang, "Active harmonic filtering using current-controlled, grid-connected DG units with closed-loop power control," *IEEE Trans. Power Electron.*, Vol. 29, No. 2, pp. 642-653, Feb. 2014.
[19] Y. Yang, F. Blaabjerg, H. Wang and M. G. Simoes, "Power control flexibilities for grid-connected multi-functional photovoltaic inverters," *IET Renewable Power Generation*, Vol. 10, No. 4, pp. 504-513, Apr. 2016.
[20] Z. Zou, Z. Wang, and M. Cheng, "Modeling, analysis, and design of multifunction grid-interfaced inverters with output LCL filter," *IEEE Trans. Power Electron.*, Vol. 29, No. 7, pp. 3830-3839, Jul. 2014.
[21] T. F. Wu, H. S. Nien, H. M. Hsieh, and C. L. Shen, "PV power injection and active power filtering with amplitude-clamping and amplitude-scaling algorithms," *IEEE Trans. Ind. Applicat.*, Vol. 43, No. 3, pp.731-741, May 2007.
[22] Z. Zeng, R. Zhao, and H. Yang, "Coordinated control of multi-functional grid-tied inverters using conductance and susceptance limitation," *IET Power Electronics*, Vol. 7, No. 7, pp. 1821-1831, Jul. 2014.
[23] Y. Yang, K. Zhou, and F. Blaabjerg, "Current harmonics from single-phase grid-connected inverters-examination and suppression," in *IEEE Journal of Emerging and Selected Topics in Power Electronics*, Vol. 4, No. 1, pp. 221-233, Mar. 2016.
[24] M. Ciobotaru, R. Teodorescu, and F. Blaabjerg, "Control of single-stage single-phase PV inverter," *Journal of European Power Electronics and Drives*, Vol 16, No 3, pp. 20-26, 2006.
[25] M. A. Rezaei, K. J. Lee, and A. Q. Huang, "A high-efficiency flyback micro-inverter with a new adaptive snubber for photovoltaic applications," *IEEE Trans. Power Electron.*, Vol. 31, No. 1, pp. 318-327, Jan. 2016.
[26] F. Chen, Q. Zhang, A. Amirahmadi, and I. Batarseh, "Modeling and analysis of dc-link voltage for three-phase four-wire two-stage micro-inverter," in *29th Annual IEEE Applied Power Electronics Conference and Exposition(APEC)*, pp. 3000-3005, May 2014.
[27] D. Chen, and L. Li, "Novel static inverters with high frequency pulse DC link," *IEEE Trans. Power Electron.*, Vol. 19, No. 4, pp. 971-978, Jul. 2004.
[28] Q. Li, and P. Wolfs, "A current fed two-inductor boost converter with an integrated magnetic structure and passive lossless snubbers for photovoltaic module integrated converter applications," *IEEE Trans. Power Electron.*, Vol. 22, No. 1, pp.309-321, Jan. 2007.
[29] A. Abramovitz, B. Zhao, and K. M. Smedley, "High-gain single-stage boosting inverter for photovoltaic applications," *IEEE Trans. Power Electron.*, Vol. 31, No. 5, pp. 3550-3558, May 2016.
[30] M. H. Karimi, H. Zamani, K. Kanzi, and Q.V. Farahani, "Implementation of a 35kVA converter base on the 3-phase 4-wire STATCOMs for medium voltage unbalanced systems," *Journal of Power Electronics*, Vol. 13, No. 5, pp.877-883, Sept. 2013.
[31] J. S. Kim, and Y. S. Kim, "A new control method for a single-phase hybrid active power filter based on a rotating reference frame," *Journal of Power Electronics,* Vol. 9, No. 5, pp. 718-725, Sep. 2009.
[32] P. C. Tan, P. C. Loh, and D. G. Holmes, "High-performance harmonic extraction algorithm for a 25kV traction power quality conditioner," in *IEE Proceedings Electric Power Applications*, Vol. 151, No.5, pp. 505-512, Sep. 2004.
[33] IEEE Recommended Practice and Requirements for Harmonic Control in Electric Power Systems, IEEE Std 519-2014 (Revision of IEEE Std 519-1992), pp. 1-29, 2014.
[34] J. T. Su and C. W. Liu, "A novel phase-shedding control scheme for improved light load efficiency of multiphase interleaved DC–DC converters," *IEEE Trans. Power Electron.,* Vol. 28, No. 10, pp. 4742-4752, Oct. 2013.
[35] Y. Ahn, I. Jeon, and J. Roh, "A multiphase Buck converter with a rotating phase-shedding scheme for efficient light-load control," *IEEE J. Solid-State Circuits*, Vol. 49, No. 11, pp. 2673-2683, Nov. 2014.
[36] H. C. Chen, "Interleaved current sensorless control for multiphase boost-type switch-mode rectifier with phase-shedding operation." *IEEE Trans. Ind. Applicat.*, Vol. 61, No. 2, pp.766-775, Feb. 2014.

Guofeng Zhu received his B.S. degree in Electrical Engineering from Tongji University, Shanghai, China, in 2010; where he is presently working towards his Ph.D. degree in Measurement Techniques and Automation. His current research interests include PV micro-inverters, power equality and power electronic converters.

Longhua Mu received his B.S., M.S., and Ph.D. degrees in Electrical Engineering from the China University of Mining and Technology, Xuzhou, China, in 1986, 1988, and 1998, respectively. He has been a Full Professor in the Department of Electrical Engineering, Tongji University, Shanghai, China, since 2004. His current research interests include protective relaying of power systems, microgrids and power quality.

Junhua Yan received his M.S. degree from the Department of Electrical Engineering and Automation from Tongji University, Shanghai, China, in 2016. He is presently working as an Engineer in the SAIC Motor Corporation Limited, Shanghai, China, where he participated in numerous projects related to the power converter in PV generation systems and the battery management systems in electric vehicles. His current research interests include power electronic converters.